Observation of D0(+) -> K-S(0)pi(0(+))eta ' and improved measurement of D-0 -> K-pi(+)eta '

BESIII Collaboration; Haddadi, Z.; Kalantar-Nayestanaki, N.; Kavatsyuk, Myroslav; Messchendorp, J. G.; Tiemens, M.

Published in:
Physical Review D

DOI:
10.1103/PhysRevD.98.092009

Publication date:
2018

Observation of $D^{0(+)} \to K^0_S \pi^{0(+)} \eta'$ and improved measurement of $D^0 \to K^- \pi^+ \eta'$

M. Ablikim,[1] M. N. Achasov,[10,d] S. Ahmed,[15] M. Albrecht,[4] M. Alekseev,[55a,55c] A. Amoroso,[55a,55c] F. F. An,[1] Q. An,[52,42] Y. Bai,[41] O. Bakina,[27] R. Baldini Ferroli,[23a] Y. Ban,[35] K. Begzsuren,[25] D. W. Bennett,[22] J. V. Bennett,[5] N. Berger,[26] M. Bertani,[23a] D. Bettoni,[24a] F. Bianchi,[55a,55c] E. Boger,[27,b] I. Boyko,[27] R. A. Briere,[5] H. Cai,[57] X. Cai,[1,42] A. Calcaterra,[23a] G. F. Cao,[1,46] S. A. Cetin,[45b] J. Chai,[55c] J. F. Chang,[1,42] W. L. Chang,[1,46] G. Chelkov,[27,b,c] G. Chen,[1] H. S. Chen,[1,46] J. C. Chen,[1] M. L. Chen,[1,42] P. L. Chen,[53] S. J. Chen,[33] X. R. Chen,[30] Y. B. Chen,[1,42] W. Cheng,[55c] X. K. Chu,[35] G. Cibinetto,[24a] F. Cossio,[55c] H. L. Dai,[1,42] J. P. Dai,[37,h] A. Dbeyssi,[15] D. Dedovich,[27] Z. Y. Deng,[1] A. Denig,[26] I. Denysenko,[27] M. Destefanis,[55a,55c] F. De Mori,[55a,55c] Y. Ding,[31] C. Dong,[34] J. Dong,[1,42] L. Y. Dong,[1,46] M. Y. Dong,[1,42,46] Z. L. Dou,[33] S. X. Du,[60] P. F. Duan,[1] J. Fang,[1,42] S. S. Fang,[1,46] Y. Fang,[1] R. Farinelli,[24a,24b] L. Fava,[55b,55c] F. Feldbauer,[4] G. Felici,[23a] C. Q. Feng,[52,42] M. Fritsch,[4] C. D. Fu,[1] Q. Gao,[1] X. L. Gao,[52,42] Y. Gao,[44] Y. G. Gao,[6] Z. Gao,[52,42] B. Garillon,[26] I. Garzia,[24a] A. Gilman,[49] K. Goetzen,[11] L. Gong,[34] W. X. Gong,[1,42] W. Gradl,[26] M. Greco,[55a,55c] L. M. Gu,[33] M. H. Gu,[1,42] Y. T. Gu,[13] A. Q. Guo,[1] L. B. Guo,[32] R. P. Guo,[1,46] Y. P. Guo,[26] A. Guskov,[27] Z. Haddadi,[29] S. Han,[57] X. Q. Hao,[16] F. A. Harris,[47] K. L. He,[1,46] F. H. Heinsius,[4] T. Held,[4] Y. K. Heng,[1,42,46] Z. L. Hou,[1] H. M. Hu,[1,46] J. F. Hu,[37,h] T. Hu,[1,42,46] Y. Hu,[1] G. S. Huang,[52,42] J. S. Huang,[16] X. T. Huang,[36] X. Z. Huang,[33] Z. L. Huang,[31] T. Hussain,[54] W. Ikegami Andersson,[56] W. Imoehl,[22] M. Irshad,[52,42] Q. Ji,[1] Q. P. Ji,[16] X. B. Ji,[1,46] X. L. Ji,[1,42] H. L. Jiang,[36] X. S. Jiang,[1,42,46] X. Y. Jiang,[34] J. B. Jiao,[36] Z. Jiao,[18] D. P. Jin,[1,42,46] S. Jin,[33] Y. Jin,[48] T. Johansson,[56] N. Kalantar-Nayestanaki,[29] X. S. Kang,[34] M. Kavatsyuk,[29] B. C. Ke,[1] I. K. Keshk,[4] T. Khan,[52,42] A. Khoukaz,[50] P. Kiese,[26] R. Kiuchi,[1] R. Kliemt,[11] L. Koch,[28] O. B. Kolcu,[45b,f] B. Kopf,[4] M. Kuemmel,[4] M. Kuessner,[4] A. Kupsc,[56] M. Kurth,[1] W. Kühn,[28] J. S. Lange,[28] P. Larin,[15] L. Lavezzi,[55c] S. Leiber,[4] H. Leithoff,[26] C. Li,[56] Cheng Li,[52,42] D. M. Li,[60] F. Li,[1,42] F. Y. Li,[35] G. Li,[1] H. B. Li,[1,46] H. J. Li,[1,46] J. C. Li,[1] J. W. Li,[40] K. J. Li,[43] Kang Li,[14] Ke Li,[1] L. K. Li,[1] Lei Li,[3] P. L. Li,[52,42] P. R. Li,[46,7] Q. Y. Li,[36] T. Li,[36] W. D. Li,[1,46] W. G. Li,[1] X. L. Li,[36] X. N. Li,[1,42] X. Q. Li,[34] Z. B. Li,[43] H. Liang,[52,42] Y. F. Liang,[39] Y. T. Liang,[28] G. R. Liao,[12] L. Z. Liao,[1,46] J. Libby,[21] C. X. Lin,[43] D. X. Lin,[15] B. Liu,[37,h] B. J. Liu,[1] C. X. Liu,[1] D. Liu,[52,42] D. Y. Liu,[37,h] F. H. Liu,[38] Fang Liu,[1] Feng Liu,[6] H. B. Liu,[13] H. L. Liu,[41] H. M. Liu,[1,46] Huanhuan Liu,[1] Huihui Liu,[17] J. B. Liu,[52,42] J. Y. Liu,[1,46] K. Y. Liu,[31] Ke Liu,[6] L. D. Liu,[35] Q. Liu,[46] S. B. Liu,[52,42] X. Liu,[30] Y. B. Liu,[34] Z. A. Liu,[1,42,46] Zhiqing Liu,[26] Y. F. Long,[35] X. C. Lou,[1,42,46] H. J. Lu,[18] J. G. Lu,[1,42] Y. Lu,[1] Y. P. Lu,[1,42] C. L. Luo,[32] M. X. Luo,[59] P. W. Luo,[43] T. Luo,[9,j] X. L. Luo,[1,42] S. Lusso,[55c] X. R. Lyu,[46] F. C. Ma,[31] H. L. Ma,[1] L. L. Ma,[36] M. M. Ma,[1,46] Q. M. Ma,[1] X. N. Ma,[34] X. Y. Ma,[1,42] Y. M. Ma,[36] F. E. Maas,[15] M. Maggiora,[55a,55c] S. Maldaner,[26] Q. A. Malik,[54] A. Mangoni,[23b] Y. J. Mao,[35] Z. P. Mao,[1] S. Marcello,[55a,55c] Z. X. Meng,[48] J. G. Messchendorp,[29] G. Mezzadri,[24a] J. Min,[1,42] T. J. Min,[33] R. E. Mitchell,[22] X. H. Mo,[1,42,46] Y. J. Mo,[6] C. Morales Morales,[15] N. Yu. Muchnoi,[10,d] H. Muramatsu,[49] A. Mustafa,[4] S. Nakhoul,[11,g] Y. Nefedov,[27] F. Nerling,[11,g] I. B. Nikolaev,[10,d] Z. Ning,[1,42] S. Nisar,[8] S. L. Niu,[1,42] X. Y. Niu,[1,46] S. L. Olsen,[46] Q. Ouyang,[1,42,46] S. Pacetti,[23b] Y. Pan,[52,42] M. Papenbrock,[56] P. Patteri,[23a] M. Pelizaeus,[4] J. Pellegrino,[55a,55c] H. P. Peng,[52,42] Z. Y. Peng,[13] K. Peters,[11,g] J. Pettersson,[56] J. L. Ping,[32] R. G. Ping,[1,46] A. Pitka,[4] R. Poling,[49] V. Prasad,[52,42] H. R. Qi,[2] M. Qi,[33] T. Y. Qi,[2] S. Qian,[1,42] C. F. Qiao,[46] N. Qin,[57] X. S. Qin,[4] Z. H. Qin,[1,42] J. F. Qiu,[1] S. Q. Qu,[34] K. H. Rashid,[54,i] C. F. Redmer,[26] M. Richter,[4] M. Ripka,[26] A. Rivetti,[55c] M. Rolo,[55c] G. Rong,[1,46] Ch. Rosner,[15] A. Sarantsev,[27,e] M. Savrié,[24b] K. Schoenning,[56] W. Shan,[19] X. Y. Shan,[52,42] M. Shao,[52,42] C. P. Shen,[2] P. X. Shen,[34] X. Y. Shen,[1,46] H. Y. Sheng,[1] X. Shi,[1,42] J. J. Song,[36] W. M. Song,[36] X. Y. Song,[1] S. Sosio,[55a,55c] C. Sowa,[4] S. Spataro,[55a,55c] F. F. Sui,[36] G. X. Sun,[1] J. F. Sun,[16] L. Sun,[57] S. S. Sun,[1,46] X. H. Sun,[1] Y. J. Sun,[52,42] Y. K. Sun,[52,42] Y. Z. Sun,[1] Z. J. Sun,[1,42] Z. T. Sun,[1] Y. T. Tan,[52,42] C. J. Tang,[39] G. Y. Tang,[1] X. Tang,[1] M. Tiemens,[29] B. Tsednee,[25] I. Uman,[45d] B. Wang,[1] B. L. Wang,[46] C. W. Wang,[33] D. Wang,[35] D. Y. Wang,[35] H. H. Wang,[36] K. Wang,[1,42] L. L. Wang,[1] L. S. Wang,[1] M. Wang,[36] Meng Wang,[1,46] P. Wang,[1] P. L. Wang,[1] W. P. Wang,[52,42] X. F. Wang,[1] Y. Wang,[52,42] Y. F. Wang,[1,42,46] Y. Q. Wang,[16] Z. Wang,[1,42] Z. G. Wang,[1,42] Z. Y. Wang,[1] Zongyuan Wang,[1,46] T. Weber,[4] D. H. Wei,[12] P. Weidenkaff,[26] S. P. Wen,[1] U. Wiedner,[4] M. Wolke,[56] L. H. Wu,[1] L. J. Wu,[1,46] Z. Wu,[1,42] L. Xia,[52,42] X. Xia,[36] Y. Xia,[20] D. Xiao,[1] Y. J. Xiao,[1,46] Z. J. Xiao,[32] Y. G. Xie,[1,42] Y. H. Xie,[6] X. A. Xiong,[1,46] Q. L. Xiu,[1,42] G. F. Xu,[1] J. J. Xu,[1,46] L. Xu,[1] Q. J. Xu,[14] X. P. Xu,[40] F. Yan,[53] L. Yan,[55a,55c] W. B. Yan,[52,42] W. C. Yan,[2] Y. H. Yan,[20] H. J. Yang,[37,h] H. X. Yang,[1] L. Yang,[57] R. X. Yang,[52,42] S. L. Yang,[1,46] Y. H. Yang,[33] Y. X. Yang,[12] Yifan Yang,[1,46] Z. Q. Yang,[20] M. Ye,[1,42] M. H. Ye,[7] J. H. Yin,[1] Z. Y. You,[43] B. X. Yu,[1,42,46] C. X. Yu,[34] J. S. Yu,[30] J. S. Yu,[20] C. Z. Yuan,[1,46] Y. Yuan,[1] A. Yuncu,[45b,a] A. A. Zafar,[54] Y. Zeng,[20] B. X. Zhang,[1] B. Y. Zhang,[1,42] C. C. Zhang,[1] D. H. Zhang,[1] H. H. Zhang,[43] H. Y. Zhang,[1,42] J. Zhang,[1,46] J. L. Zhang,[58] J. Q. Zhang,[4] J. W. Zhang,[1,42,46] J. Y. Zhang,[1] J. Z. Zhang,[1,46] K. Zhang,[1,46] L. Zhang,[44] S. F. Zhang,[33] T. J. Zhang,[37,h] X. Y. Zhang,[36] Y. Zhang,[52,42] Y. H. Zhang,[1,42] Y. T. Zhang,[52,42] Yang Zhang,[1] Yao Zhang,[1] Yu Zhang,[46] Z. H. Zhang,[6] Z. P. Zhang,[52] Z. Y. Zhang,[57] G. Zhao,[1] J. W. Zhao,[1,42] J. Y. Zhao,[1,46] J. Z. Zhao,[1,42] Lei Zhao,[52,42] Ling Zhao,[1] M. G. Zhao,[34] Q. Zhao,[1] S. J. Zhao,[60] T. C. Zhao,[1] Y. B. Zhao,[1,42] Z. G. Zhao,[52,42] A. Zhemchugov,[27,b] B. Zheng,[53]

J. P. Zheng,[1,42] W. J. Zheng,[36] Y. H. Zheng,[46] B. Zhong,[32] L. Zhou,[1,42] Q. Zhou,[1,46] X. Zhou,[57] X. K. Zhou,[52,42] X. R. Zhou,[52,42] X. Y. Zhou,[1] Xiaoyu Zhou,[20] Xu Zhou,[20] A. N. Zhu,[1,46] J. Zhu,[34] J. Zhu,[43] K. Zhu,[1] K. J. Zhu,[1,42,46] S. Zhu,[1] S. H. Zhu,[51] X. L. Zhu,[44] Y. C. Zhu,[52,42] Y. S. Zhu,[1,46] Z. A. Zhu,[1,46] J. Zhuang,[1,42] B. S. Zou,[1] and J. H. Zou[1]

(BESIII Collaboration)

[1]*Institute of High Energy Physics, Beijing 100049, People's Republic of China*
[2]*Beihang University, Beijing 100191, People's Republic of China*
[3]*Beijing Institute of Petrochemical Technology, Beijing 102617, People's Republic of China*
[4]*Bochum Ruhr-University, D-44780 Bochum, Germany*
[5]*Carnegie Mellon University, Pittsburgh, Pennsylvania 15213, USA*
[6]*Central China Normal University, Wuhan 430079, People's Republic of China*
[7]*China Center of Advanced Science and Technology, Beijing 100190, People's Republic of China*
[8]*COMSATS Institute of Information Technology, Lahore, Defence Road, Off Raiwind Road, 54000 Lahore, Pakistan*
[9]*Fudan University, Shanghai 200443, People's Republic of China*
[10]*G.I. Budker Institute of Nuclear Physics SB RAS (BINP), Novosibirsk 630090, Russia*
[11]*GSI Helmholtzcentre for Heavy Ion Research GmbH, D-64291 Darmstadt, Germany*
[12]*Guangxi Normal University, Guilin 541004, People's Republic of China*
[13]*Guangxi University, Nanning 530004, People's Republic of China*
[14]*Hangzhou Normal University, Hangzhou 310036, People's Republic of China*
[15]*Helmholtz Institute Mainz, Johann-Joachim-Becher-Weg 45, D-55099 Mainz, Germany*
[16]*Henan Normal University, Xinxiang 453007, People's Republic of China*
[17]*Henan University of Science and Technology, Luoyang 471003, People's Republic of China*
[18]*Huangshan College, Huangshan 245000, People's Republic of China*
[19]*Hunan Normal University, Changsha 410081, People's Republic of China*
[20]*Hunan University, Changsha 410082, People's Republic of China*
[21]*Indian Institute of Technology Madras, Chennai 600036, India*
[22]*Indiana University, Bloomington, Indiana 47405, USA*
[23a]*INFN Laboratori Nazionali di Frascati, I-00044, Frascati, Italy*
[23b]*INFN and University of Perugia, I-06100, Perugia, Italy*
[24a]*INFN Sezione di Ferrara, I-44122, Ferrara, Italy*
[24b]*University of Ferrara, I-44122, Ferrara, Italy*
[25]*Institute of Physics and Technology, Peace Ave. 54B, Ulaanbaatar 13330, Mongolia*
[26]*Johannes Gutenberg University of Mainz, Johann-Joachim-Becher-Weg 45, D-55099 Mainz, Germany*
[27]*Joint Institute for Nuclear Research, 141980 Dubna, Moscow region, Russia*
[28]*Justus-Liebig-Universitaet Giessen, II. Physikalisches Institut, Heinrich-Buff-Ring 16, D-35392 Giessen, Germany*
[29]*KVI-CART, University of Groningen, NL-9747 AA Groningen, The Netherlands*
[30]*Lanzhou University, Lanzhou 730000, People's Republic of China*
[31]*Liaoning University, Shenyang 110036, People's Republic of China*
[32]*Nanjing Normal University, Nanjing 210023, People's Republic of China*
[33]*Nanjing University, Nanjing 210093, People's Republic of China*
[34]*Nankai University, Tianjin 300071, People's Republic of China*
[35]*Peking University, Beijing 100871, People's Republic of China*
[36]*Shandong University, Jinan 250100, People's Republic of China*
[37]*Shanghai Jiao Tong University, Shanghai 200240, People's Republic of China*
[38]*Shanxi University, Taiyuan 030006, People's Republic of China*
[39]*Sichuan University, Chengdu 610064, People's Republic of China*
[40]*Soochow University, Suzhou 215006, People's Republic of China*
[41]*Southeast University, Nanjing 211100, People's Republic of China*
[42]*State Key Laboratory of Particle Detection and Electronics, Beijing 100049, Hefei 230026, People's Republic of China*
[43]*Sun Yat-Sen University, Guangzhou 510275, People's Republic of China*
[44]*Tsinghua University, Beijing 100084, People's Republic of China*
[45a]*Ankara University, 06100 Tandogan, Ankara, Turkey*
[45b]*Istanbul Bilgi University, 34060 Eyup, Istanbul, Turkey*
[45c]*Uludag University, 16059 Bursa, Turkey*
[45d]*Near East University, Nicosia, North Cyprus, Mersin 10, Turkey*

[46]University of Chinese Academy of Sciences, Beijing 100049, People's Republic of China
[47]University of Hawaii, Honolulu, Hawaii 96822, USA
[48]University of Jinan, Jinan 250022, People's Republic of China
[49]University of Minnesota, Minneapolis, Minnesota 55455, USA
[50]University of Muenster, Wilhelm-Klemm-Str. 9, 48149 Muenster, Germany
[51]University of Science and Technology Liaoning, Anshan 114051, People's Republic of China
[52]University of Science and Technology of China, Hefei 230026, People's Republic of China
[53]University of South China, Hengyang 421001, People's Republic of China
[54]University of the Punjab, Lahore-54590, Pakistan
[55a]University of Turin, I-10125, Turin, Italy
[55b]University of Eastern Piedmont, I-15121, Alessandria, Italy
[55c]INFN, I-10125, Turin, Italy
[56]Uppsala University, Box 516, SE-75120 Uppsala, Sweden
[57]Wuhan University, Wuhan 430072, People's Republic of China
[58]Xinyang Normal University, Xinyang 464000, People's Republic of China
[59]Zhejiang University, Hangzhou 310027, People's Republic of China
[60]Zhengzhou University, Zhengzhou 450001, People's Republic of China

(Received 11 September 2018; published 14 November 2018)

By analyzing an e^+e^- data sample corresponding to an integrated luminosity of 2.93 fb^{-1} taken at a center-of-mass energy of 3.773 GeV with the BESIII detector, we measure the branching fractions of the Cabibbo-favored hadronic decays $D^0 \to K^-\pi^+\eta'$, $D^0 \to K^0_S\pi^0\eta'$, and $D^+ \to K^0_S\pi^+\eta'$, which are determined to be $(6.43 \pm 0.15_{\mathrm{stat}} \pm 0.31_{\mathrm{syst}}) \times 10^{-3}$, $(2.52 \pm 0.22_{\mathrm{stat}} \pm 0.15_{\mathrm{syst}}) \times 10^{-3}$, and $(1.90 \pm 0.17_{\mathrm{stat}} \pm 0.13_{\mathrm{syst}}) \times 10^{-3}$, respectively. The precision of the branching fraction of $D^0 \to K^-\pi^+\eta'$ is significantly improved, and the processes $D^0 \to K^0_S\pi^0\eta'$ and $D^+ \to K^0_S\pi^+\eta'$ are observed for the first time.

DOI: 10.1103/PhysRevD.98.092009

I. INTRODUCTION

Hadronic decays of D mesons provide important information to understand the weak and strong interactions in the charm sector. Various experiments have measured the branching fractions of hadronic decays of D mesons [1]. However, the measurement accuracy of the Cabibbo-favored (CF) decays $D \to \bar{K}\pi\eta'$ is still very poor [1]. The Particle Data Group (PDG) gives a branching fraction of $(0.75 \pm 0.19)\%$ for $D^0 \to K^-\pi^+\eta'$, which was measured by the CLEO collaboration 25 years ago [1,2]. There are no measurements for the isospin-related decay modes $D^0 \to K^0_S\pi^0\eta'$ and $D^+ \to K^0_S\pi^+\eta'$. The statistical isospin model (SIM) proposed in Refs. [3,4] predicts a simple ratio of the branching fractions for the isospin multiplets: $\mathcal{B}(D^0 \to K^-\pi^+\eta') : \mathcal{B}(D^0 \to K^0_S\pi^0\eta') : \mathcal{B}(D^+ \to K^0_S\pi^+\eta') \equiv 1 : \mathcal{R}^0 : \mathcal{R}^+ \equiv 1 : \frac{\mathcal{B}(D^0 \to K^0_S\pi^0\eta')}{\mathcal{B}(D^0 \to K^-\pi^+\eta')} : \frac{\mathcal{B}(D^+ \to K^0_S\pi^+\eta')}{\mathcal{B}(D^0 \to K^-\pi^+\eta')} = 1 : 0.4 : 0.9$. Precision measurements of the branching fractions of $D \to \bar{K}\pi\eta'$ are crucial to test the SIM prediction.

In this paper, we report an improved measurement of the branching fraction for $D^0 \to K^-\pi^+\eta'$ and the first measurements of the branching fractions for $D^0 \to K^0_S\pi^0\eta'$ and $D^+ \to K^0_S\pi^+\eta'$. The analysis is performed using an e^+e^- annihilation data sample corresponding to an integrated luminosity of 2.93 fb^{-1} [5] collected with the BESIII detector [6] at $\sqrt{s} = 3.773$ GeV. At this energy, relatively clean D^0 and D^+ meson samples are obtained from the processes $e^+e^- \to \psi(3770) \to D^0\bar{D}^0$ or D^+D^-. To improve statistics, we use a single-tag method, in which either a D or $\bar{D}$ is reconstructed in an event. Throughout the

[a]Also at Bogazici University, 34342 Istanbul, Turkey.
[b]Also at the Moscow Institute of Physics and Technology, Moscow 141700, Russia.
[c]Also at the Functional Electronics Laboratory, Tomsk State University, Tomsk, 634050, Russia.
[d]Also at the Novosibirsk State University, Novosibirsk, 630090, Russia.
[e]Also at the NRC "Kurchatov Institute", PNPI, 188300, Gatchina, Russia.
[f]Also at Istanbul Arel University, 34295 Istanbul, Turkey.
[g]Also at Goethe University Frankfurt, 60323 Frankfurt am Main, Germany.
[h]Also at Key Laboratory for Particle Physics, Astrophysics and Cosmology, Ministry of Education; Shanghai Key Laboratory for Particle Physics and Cosmology; Institute of Nuclear and Particle Physics, Shanghai 200240, People's Republic of China.
[i]Also at Government College Women University, Sialkot—51310. Punjab, Pakistan.
[j]Also at Key Laboratory of Nuclear Physics and Ion-beam Application (MOE) and Institute of Modern Physics, Fudan University, Shanghai 200443, People's Republic of China.

text, charge conjugated modes are implied, and $D\bar{D}$ refers to $D^0\bar{D}^0$ and D^+D^- unless stated explicitly.

II. BESIII DETECTOR AND MONTE CARLO SIMULATION

The BESIII detector is a magnetic spectrometer that operates at the BEPCII collider. It has a cylindrical geometry with a solid-angle coverage of 93% of 4π. It consists of several main components. A 43-layer main drift chamber (MDC) surrounding the beam pipe performs precise determinations of charged particle trajectories and measures the specific ionization energy loss ($\mathrm{d}E/\mathrm{d}x$) for charged particle identification (PID). An array of time-of-flight counters (TOF) is located outside the MDC and provides additional PID information. A CsI(Tl) electromagnetic calorimeter (EMC) surrounds the TOF and is used to measure the deposited energies of photons and electrons. A solenoidal superconducting magnet outside the EMC provides a 1 T magnetic field in the central tracking region of the detector. The iron flux return of the magnet is instrumented with the resistive plate muon counters arranged in nine layers in the barrel and eight layers in the endcaps for identification of muons with momenta greater than 0.5 GeV/c. More details about the BESIII detector are described in Ref. [6].

A Monte Carlo (MC) simulation software package, based on GEANT4 [7], includes the geometric description and response of the detector and is used to determine the detection efficiency and to estimate backgrounds for each decay mode. An inclusive MC sample, which includes the $D^0\bar{D}^0$, D^+D^- and non-$D\bar{D}$ decays of the $\psi(3770)$, initial-state-radiation (ISR) production of the $\psi(3686)$ and J/ψ, the continuum process $e^+e^- \to q\bar{q}$ ($q = u, d, s$), Bhabha scattering events, dimuon events, and ditau events, is produced at $\sqrt{s} = 3.773$ GeV. The equivalent luminosity of the inclusive MC sample is ten times that of the data sample. The $\psi(3770)$ decays are generated with the MC generator KKMC [8], which incorporates the effects of ISR [9]. Final-state-radiation (FSR) effects are simulated with the PHOTOS package [10]. The known decay modes are generated using EVTGEN [11] with branching fractions taken from the PDG [1], while the remaining unknown decays are generated using LUNDCHARM [12].

III. EVENT SELECTION

In this analysis, all charged tracks are required to be within $|\cos\theta| < 0.93$, where θ is the polar angle with respect to the positron beam. Good charged tracks, except those used to reconstruct K^0_S mesons, are required to originate from the interaction region defined by $V_{xy} < 1$ cm and $|V_z| < 10$ cm, where V_{xy} and $|V_z|$ are the distances of the closest approach of the reconstructed tracks to the interaction point (IP), perpendicular to and along the beam direction, respectively.

Charged kaons and pions are identified using the $\mathrm{d}E/\mathrm{d}x$ and TOF measurements. The combined confidence levels for the kaon and pion hypotheses (CL_K and CL_π) are calculated and the charged track is identified as kaon (pion) if $CL_{K(\pi)}$ is greater than $CL_{\pi(K)}$.

The neutral kaon is reconstructed via the $K^0_S \to \pi^+\pi^-$ decay mode. Two oppositely charged tracks with $|V_z| < 20$ cm are assumed to be a $\pi^+\pi^-$ pair without PID requirements and the $\pi^+\pi^-$ pair is constrained to originate from a common vertex. The $\pi^+\pi^-$ combination with an invariant mass $M_{\pi^+\pi^-}$ in the range $|M_{\pi^+\pi^-} - M_{K^0_S}| < 0.012$ GeV/c^2, where $M_{K^0_S}$ is the nominal K^0_S mass [1], and a measured flight distance from the IP greater than twice its resolution is accepted as a K^0_S candidate. Figure 1(a) shows the $\pi^+\pi^-$ invariant mass distribution, where the two solid arrows denote the K^0_S signal region.

Photon candidates are selected using the EMC information. The time of the candidate shower must be within 700 ns of the event start time and the shower energy should be greater than 25 (50) MeV if the crystal with the maximum deposited energy for the cluster of interest is in the barrel (endcap) region [6]. The opening angle between the candidate shower and any charged track is required to be greater than 10° to eliminate showers associated with charged tracks. Both π^0 and η mesons are reconstructed via the $\gamma\gamma$ decay mode. The $\gamma\gamma$ combination with an invariant mass within (0.115,0.150) or $(0.515, 0.570)$ GeV/c^2 is regarded as a π^0 or η candidate, respectively. To improve resolution, a one constraint (1-C) kinematic fit is applied to constrain the invariant mass of the photon pair to the nominal π^0 or η invariant mass [1].

The η' mesons are reconstructed through the decay $\eta' \to \pi^+\pi^-\eta$. The invariant mass of the $\pi^+\pi^-\eta$ combination $M_{\pi^+\pi^-\eta}$ is required to satisfy $|M_{\pi^+\pi^-\eta} - M_{\eta'}| < 0.015$GeV/$c^2$, where $M_{\eta'}$ is the nominal η' mass [1]. The boundaries of the one dimensional (1D) η' signal region are illustrated by the two solid arrows shown in Fig. 1(b). The $D^{0(+)} \to K^-(K^0_S)\pi^+\eta'$ decay is selected from the $K^-(K^0_S)\pi^+\pi^+\pi^-\eta$ combination. Since the two π^+s in the event have low momenta and are indistinguishable, the η' may be formed from either of the $\pi^+\pi^-\eta$ combinations, whose invariant masses are denoted as $M_{\pi^+_1\pi^-\eta}$ and $M_{\pi^+_2\pi^-\eta}$. Figure 1(c) shows the scatter plot of $M_{\pi^+_2\pi^-\eta}$ versus $M_{\pi^+_1\pi^-\eta}$ for the $D^0 \to K^-\pi^+\eta'$ candidate events in the data sample. Events with at least one $\pi^+\pi^-\eta$ combination in the two dimensional (2D) η' signal region, shown by the solid lines in Fig. 1(c), are kept for further analysis.

To distinguish D mesons from backgrounds, we define two kinematic variables, the energy difference $\Delta E \equiv E_D - E_{\mathrm{beam}}$ and the beam-constrained mass $M_{\mathrm{BC}} \equiv \sqrt{E^2_{\mathrm{beam}} - |\vec{p}_D|^2}$, where E_D and $\vec{p}_D$ are the energy and momentum of the D candidate in the e^+e^- center-of-mass

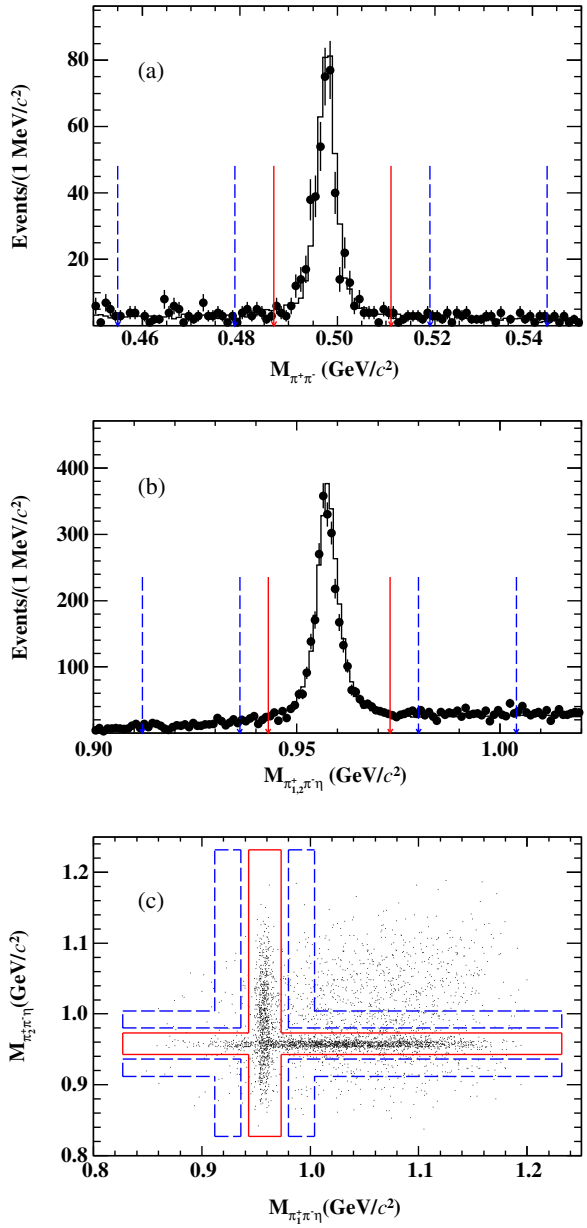

FIG. 1. (a) Distribution of $M_{\pi^+\pi^-}$ for the K^0_S candidates from $D^0 \to K^0_S\pi^0\eta'$ decays and (b) the combined $M_{\pi^+_1\pi^-\eta}$ and $M_{\pi^+_2\pi^-\eta}$ distribution for the η' candidates from $D^0 \to K^-\pi^+\eta'$ decays, where the dots with error bars are data, the histograms are inclusive MC samples, and the pairs of red solid (blue dashed) arrows show the boundaries of the K^0_S or η' 1D signal (sideband) region. (c) Scatter plot of $M_{\pi^+_2\pi^-\eta}$ versus $M_{\pi^+_1\pi^-\eta}$ for the $D^0 \to K^-\pi^+\eta'$ candidate events in the data sample, where the range surrounded by the red solid (blue dashed) lines denotes the η' 2D signal (sideband) region. In these figures, except for the K^0_S or η' mass requirement, all selection criteria and an additional requirement of $|M_{\rm BC} - M_D| < 0.005$ GeV/c^2 have been imposed. The signal and sideband regions, illustrated here, are applied for all decays of interest in the analysis.

TABLE I. ΔE requirements, input quantities and results for the determination of the branching fractions. The efficiencies do not include the branching fractions for the decays of the daughter particles of η', η, K^0_S, and π^0 mesons. The uncertainties are statistical only.

Decay mode	ΔE (MeV)	$N_{\rm tag}$	ϵ (%)	$\mathcal{B}$ ($\times 10^{-3}$)
$D^0 \to K^-\pi^+\eta'$	$(-26, +28)$	2528 ± 59	10.97 ± 0.08	6.43 ± 0.15
$D^0 \to K^0_S\pi^0\eta'$	$(-35, +38)$	289 ± 26	4.67 ± 0.04	2.52 ± 0.22
$D^+ \to K^0_S\pi^+\eta'$	$(-27, +28)$	267 ± 24	7.23 ± 0.05	1.90 ± 0.17

system and $E_{\rm beam}$ is the beam energy. For each signal decay mode, only the combination with the minimum $|\Delta E|$ is kept if more than one candidate passes the selection requirements. Mode-dependent ΔE requirements, as listed in Table I, are applied to suppress combinatorial backgrounds. These requirements are about $\pm 3.5\sigma_{\Delta E}$ around the fitted ΔE peaks, where $\sigma_{\Delta E}$ is the resolution of the ΔE distribution obtained from fits to the data sample.

IV. DATA ANALYSIS

The $M_{\rm BC}$ distributions of the accepted candidate events for the decays of interest in the data sample are shown in Fig. 2. Unbinned maximum likelihood fits to these spectra are performed to obtain the D signal yields. In the fits, the D signal is modeled by an MC-simulated shape convolved with a Gaussian function with free parameters accounting for the difference between the detector resolution of the data and that of the MC simulation. The background shape is described by an ARGUS function [13]. The potential peaking backgrounds are investigated as follows. The combinatorial $\pi^+\pi^-$ (called BKGI) or $\pi^+\pi^-\eta$ (called BKGII) pairs in the K^0_S or η' signal region may survive the event selection criteria and form peaking backgrounds around the D mass in the $M_{\rm BC}$ distributions. These background components are validated by the data events in the $K^0_S(\eta')$ sideband region defined as $0.020(0.022) < |M_{\pi^+\pi^-(\pi^+\pi^-\eta)} - M_{K^0_S(\eta')}| < 0.044(0.046)$ GeV/c^2, as indicated by the ranges between the adjacent pair of blue dashed arrows in Fig. 1(a)[(b)]. For $D^0 \to K^-\pi^+\eta'$ and $D^+ \to K^0_S\pi^+\eta'$ decays, the data events in the η' 2D sideband region, enclosed by the blue dashed lines in Fig. 1(c), are examined. For these events, either $M_{\pi^+_1\pi^-\eta}$ or $M_{\pi^+_2\pi^-\eta}$ is in the η' 1D sideband region, but both are outside the η' 1D signal region. These two background components are normalized by the ratios of the magnitude of the backgrounds in the $K^0_S(\eta')$ signal and sideband regions. The background components from other processes (called BKGIII) are estimated by analyzing the inclusive MC sample. The scaled $M_{\rm BC}$ distributions of the surviving events for the BKGI, BKGII, and BKGIII components are

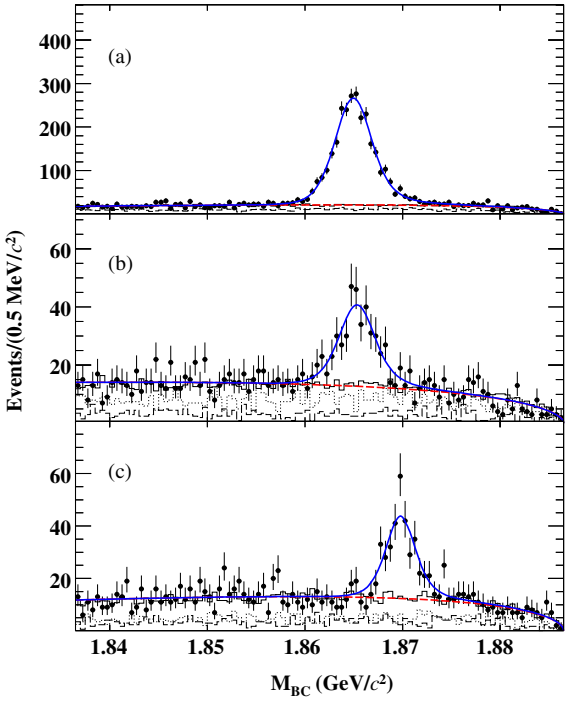

FIG. 2. Fits to the $M_{\rm BC}$ distributions of the (a) $D^0 \to K^-\pi^+\eta'$, (b) $D^0 \to K^0_S\pi^0\eta'$, and (c) $D^+ \to K^0_S\pi^+\eta'$ candidate events. The dots with error bars are data, the blue solid curves are the total fits and the red dashed curves are the fitted backgrounds. The dotted, dashed and solid histograms are the scaled BKGI, BKGII, and BKGIII components (see the last paragraph of Sec. III), respectively.

shown as the dotted, dashed, and solid histograms in Fig. 2, respectively. In these spectra, no peaking backgrounds are found, which indicates that the background shape is well modeled by the ARGUS function. From each fit, we obtain the number of $D \to \bar{K}\pi\eta'$ signal events $N_{\rm tag}$, as summarized in Table I. The statistical significances of these decays, which are estimated from the likelihood difference between the fits with and without the signal component, are all greater than 10σ.

Figure 3 shows the $M_{K\pi}$, $M_{\pi\eta'}$, and $M_{K\eta'}$ distributions of $D \to \bar{K}\pi\eta'$ candidate events for data and MC simulations after requiring $|M_{\rm BC} - M_D| < 0.005$ GeV/c^2. No obvious subresonances have been observed in these invariant mass distributions. Nevertheless, the phase space (PHSP) MC distributions are not in good agreement with the data distribution (see the blue dashed histograms and dots with errors in Fig. 3). To solve this problem, we modify the MC generator to produce the correct invariant mass distributions according to the Dalitz plot distributions in data. In the Dalitz plot, the background component is modeled by the inclusive MC simulation, while the signal component is generated according to efficiency-corrected PHSP MC simulation. In Fig. 4, we show the Dalitz plots of $D^0 \to K^-\pi^+\eta'$ candidate events for data and the modified MC sample. The invariant mass distributions $M_{K\pi}$, $M_{\pi\eta'}$, and $M_{K\eta'}$ of the modified MC samples are in good agreement with the data distributions (see the red solid histograms and

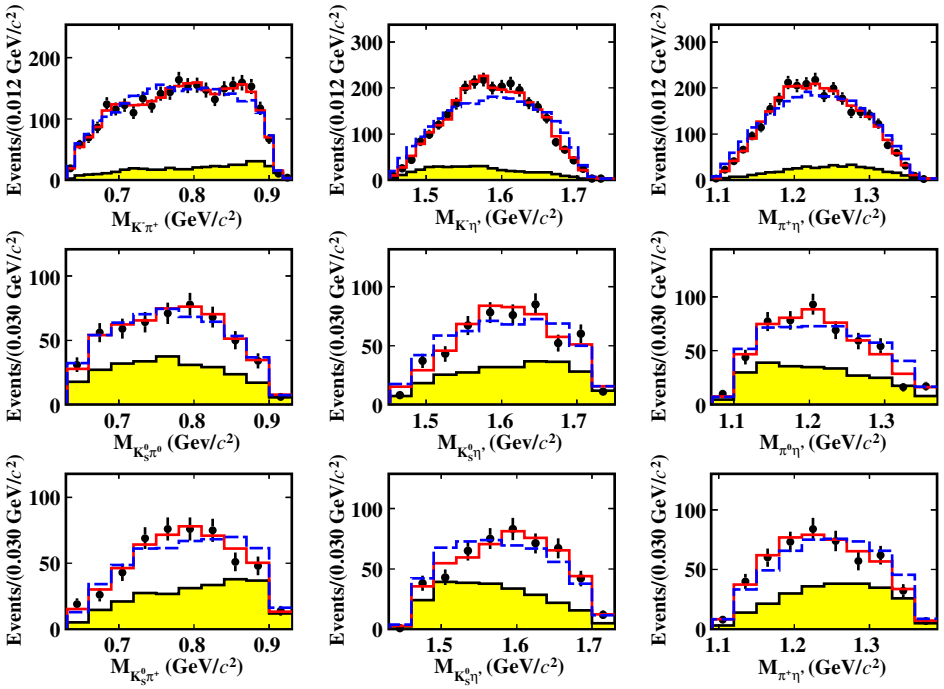

FIG. 3. The $M_{K\pi}$, $M_{\pi\eta'}$, and $M_{K\eta'}$ distributions of data (dots with error bars) and MC simulations (histograms). The top, middle, and bottom rows correspond to $D^0 \to K^-\pi^+\eta'$, $D^0 \to K^0_S\pi^0\eta'$, and $D^+ \to K^0_S\pi^+\eta'$ candidate events, respectively. The blue dashed histograms are PHSP MC samples. The red solid histograms are the modified MC samples. The yellow shaded histograms are the backgrounds estimated from the inclusive MC sample. An additional requirement of $|M_{\rm BC} - M_D| < 0.005$ GeV/c^2 has been imposed on the events shown in these plots.

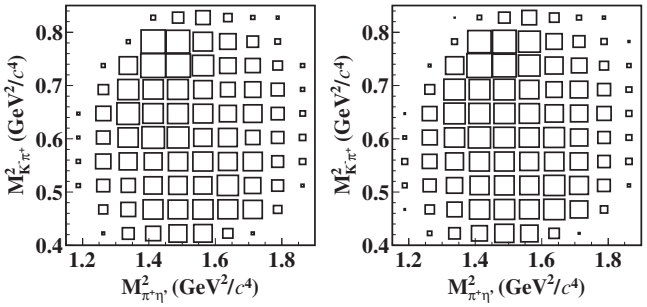

FIG. 4. Dalitz plots of $M^2_{K^-\pi^+}$ vs $M^2_{\pi^+\eta'}$ for $D^0 \to K^-\pi^+\eta'$ candidate events in data (left) and modified MC sample (right).

dots with errors in Fig. 3). In the following, we use the modified MC sample to determine the detection efficiencies in the calculation of the branching fractions.

V. BRANCHING FRACTIONS

The branching fraction of $D \to \bar{K}\pi\eta'$ is determined according to

$$\mathcal{B}(D \to \bar{K}\pi\eta') = \frac{N_{\rm tag}}{2 \cdot N_{D\bar{D}} \cdot \epsilon \cdot \mathcal{B}_{\eta'} \cdot \mathcal{B}_{\eta}(\cdot\mathcal{B}_{\rm inter})}, \quad (1)$$

where $N_{\rm tag}$ is the number of $D \to \bar{K}\pi\eta'$ signal events, $N_{D\bar{D}}$ is the total number of $D\bar{D}$ pairs, ϵ is the detection efficiency which has been corrected by the differences in the efficiencies for charged particle tracking and PID, as well as π^0 and η reconstruction, between the data and MC simulation as discussed in Sec. IV, and summarized in Table I. In Eq. (1), $\mathcal{B}_{\rm inter}$ is the product branching fraction $\mathcal{B}_{K^0_S} \cdot \mathcal{B}_{\pi^0}$ ($\mathcal{B}_{K^0_S}$) for the decay $D^0 \to K^0_S\pi^0\eta'$ ($D^+ \to K^0_S\pi^+\eta'$), and $\mathcal{B}_{\eta'}$, $\mathcal{B}_{\eta}$, $\mathcal{B}_{K^0_S}$ and $\mathcal{B}_{\pi^0}$ denote the branching fractions of the decays $\eta' \to \pi^+\pi^-\eta$, $\eta \to \gamma\gamma$, $K^0_S \to \pi^+\pi^-$, and $\pi^0 \to \gamma\gamma$, respectively, taken from the PDG [1]. With the single-tag method, the CF decays $D^0(D^+) \to \bar{K}\pi\eta'$ are indistinguishable from the doubly Cabibbo-suppressed (DCS) decays $\bar{D}^0(D^+) \to \bar{K}(K)\pi\eta'$. However, the DCS contributions are expected to be small and negligible in the calculations of branching fractions, but will be taken into account as a systematic uncertainty.

Taking $N_{D^0\bar{D}^0} = (10597 \pm 28_{\rm stat} \pm 98_{\rm syst}) \times 10^3$ and $N_{D^+D^-} = (8296 \pm 31_{\rm stat} \pm 65_{\rm syst}) \times 10^3$ from Ref. [14], the branching fraction of each decay is determined with Eq. (1) and summarized in Table I.

VI. SYSTEMATIC UNCERTAINTIES

The systematic uncertainties in the measurements of the branching fractions and the branching ratios, $\mathcal{R}^0 \equiv \frac{\mathcal{B}(D^0\to K^0_S\pi^0\eta')}{\mathcal{B}(D^0\to K^-\pi^+\eta')}$, and $\mathcal{R}^+ \equiv \frac{\mathcal{B}(D^+\to K^0_S\pi^+\eta')}{\mathcal{B}(D^0\to K^-\pi^+\eta')}$, are summarized in Table II. Each contribution, estimated relative to the measured branching fraction, is discussed below.

(i) *Number of $D\bar{D}$ pairs*: The total numbers of $D^0\bar{D}^0$ and D^+D^- pairs produced in the data sample are cited from a previous measurement [14] that uses a combined analysis of both single-tag and double-tag events in the same data sample. The total uncertainty in the quoted number of $D^0\bar{D}^0(D^+D^-)$ pairs is 1.0% (0.9%), obtained by adding both the statistical and systematic uncertainties in quadrature.

(ii) *Tracking and PID of $K^\pm(\pi^\pm)$*: The tracking and PID efficiencies for $K^\pm(\pi^\pm)$ are investigated using double-tag $D\bar{D}$ hadronic events. A small difference between the efficiency in the data sample and that in MC simulation (called the data-MC difference)

TABLE II. Relative systematic uncertainties (in %) in the branching fractions, $\mathcal{R}^0$, and $\mathcal{R}^+$. The numbers before or after '/' in the last two columns denote the remaining systematic uncertainties of $\mathcal{B}(D^0 \to K^-\pi^+\eta')$ and $\mathcal{B}(D^{0(+)} \to K^0_S\pi^{0(+)}\eta')$ that do not cancel in the determination of $\mathcal{R}^0$ and $\mathcal{R}^+$.

Source	$\mathcal{B}(D^0 \to K^-\pi^+\eta')$	$\mathcal{B}(D^0 \to K^0_S\pi^0\eta')$	$\mathcal{B}(D^+ \to K^0_S\pi^+\eta')$	$\mathcal{R}^0$	$\mathcal{R}^+$
Number of $D\bar{D}$ pairs	1.0	1.0	0.9	-/-	1.0/0.9
Tracking of $K^\pm(\pi^\pm)$	3.0	2.0	2.5	1.0/-	1.0/-
PID of $K^\pm(\pi^\pm)$	2.0	1.0	1.5	1.0/-	0.5/-
K^0_S reconstruction	…	1.5	1.5	-/1.5	-/1.5
$\pi^0(\eta)$ reconstruction	1.0	2.0	1.0	-/1.0	-/-
$M_{\rm BC}$ fit	0.5	3.6	1.9	0.5/3.6	0.5/1.9
η' mass window	1.0	1.0	1.0	-/-	-/-
ΔE requirement	0.1	2.4	4.5	0.1/2.4	0.1/4.5
MC modeling	1.6	0.5	1.7	1.6/0.5	1.6/1.7
MC statistics	0.7	0.9	0.7	0.7/0.9	0.7/0.7
Quoted branching fractions	1.7	1.7	1.7	-/0.1	-/0.1
$D^0\bar{D}^0$ mixing	0.1	0.1	…	-/-	-/-
DCS contribution	0.6	0.6	0.6	-/-	-/-
Total	4.8	6.0	6.6	5.3	6.0

is found. The momentum weighted data-MC differences in the tracking [PID] efficiencies are determined to be $(+2.4 \pm 0.4)\%$, $(+1.0 \pm 0.5)\%$, and $(+1.9 \pm 1.0)\%$ [$(-0.2 \pm 0.1)\%$, $(-0.1 \pm 0.1)\%$ and $(-0.2 \pm 0.1)\%$] for $K^{\pm}$, $\pi^{\pm}_{\rm direct}$, and $\pi^{\pm}_{\rm in-direct}$, respectively. Here, the uncertainties are statistical and the subscript $_{\rm direct}$ or $_{\rm in-direct}$ indicates the $\pi^{\pm}$ produced in D or η' decays, respectively. In this work, the MC efficiencies have been corrected by the momentum weighted data–MC differences in the $K^{\pm}(\pi^{\pm})$ tracking and PID efficiencies. Finally, a systematic uncertainty for charged particle tracking is assigned to be 1.0% per $\pi^{\pm}_{\rm in-direct}$ and 0.5% per $K^{\pm}$ or $\pi^{\pm}_{\rm direct}$. The systematic uncertainty for PID efficiency is taken as 0.5% per $K^{\pm}$, $\pi^{\pm}_{\rm direct}$ or $\pi^{\pm}_{\rm in-direct}$.

(iii) K^0_S *reconstruction*: The K^0_S reconstruction efficiency, which includes effects from the track reconstruction of the charged pion pair, vertex fit, decay length requirement and K^0_S mass window, has been studied with a control sample of $J/\psi \to K^*(892)^{\mp}K^{\pm}$ and $J/\psi \to \phi K^0_S K^{\pm}\pi^{\mp}$ [15]. The associated systematic uncertainty is assigned as 1.5% per K^0_S.

(iv) $\pi^0(\eta)$ *reconstruction*: The π^0 reconstruction efficiency, which includes effects from the photon selection, 1-C kinematic fit and π^0 mass window, is verified with double-tag $D\bar{D}$ hadronic decay samples of $D^0 \to K^-\pi^+$, $K^-\pi^+\pi^+\pi^-$ versus $\bar{D}^0 \to K^+\pi^-\pi^0$, $K^0_S\pi^0$ [16]. A small data-MC difference in the π^0 reconstruction efficiency is found. The momentum weighted data-MC difference in π^0 reconstruction efficiencies is found to be $(-0.5 \pm 1.0)\%$, where the uncertainty is statistical. After correcting the MC efficiencies by the momentum weighted data-MC difference in π^0 reconstruction efficiency, the systematic uncertainty due to π^0 reconstruction is assigned as 1.0% per π^0. The systematic uncertainty due to η reconstruction is assumed to be the same as that for π^0 reconstruction.

(v) η' *mass window*: The uncertainty due to the η' mass window is studied by fitting to the $\pi^+\pi^-\eta$ invariant mass spectrum of the $K^-\pi^+\eta'$ candidates. The difference between the data and MC simulation in the efficiency of the η' mass window restriction is $(0.8 \pm 0.2)\%$. The associated systematic uncertainty is assigned as 1.0%.

(vi) $M_{\rm BC}$ *fit*: To estimate the systematic uncertainty due to the $M_{\rm BC}$ fit, we repeat the measurements by varying the fit range [$(1.8415, 1.8865)$ GeV/c^2], the signal shape (with different MC matching requirements) and the endpoint (1.8865 GeV/c^2) of the ARGUS function (± 0.2 MeV/c^2). Summing the relative changes in the branching fractions for these three sources in quadrature yields 0.5%, 3.6%, and 1.9% for $D^0 \to K^-\pi^+\eta'$, $D^0 \to K^0_S\pi^0\eta'$, and $D^+ \to K^0_S\pi^+\eta'$, respectively, which are assigned as systematic uncertainties.

(vii) ΔE *requirement*: To investigate the systematic uncertainty due to the ΔE requirement, we repeat the measurements with alternative ΔE requirements of $3.0\sigma_{\Delta E}$ and $4.0\sigma_{\Delta E}$ around the fitted ΔE peaks. The changes in the branching fractions, 0.1%, 2.4%, and 4.5%, are taken as systematic uncertainties for $D^0 \to K^-\pi^+\eta'$, $D^0 \to K^0_S\pi^0\eta'$, and $D^+ \to K^0_S\pi^+\eta'$, respectively.

(viii) *MC modeling*: The systematic uncertainty in the MC modeling is studied by varying MC-simulated background sizes for the input $M^2_{K\pi}$ and $M^2_{\pi\eta'}$ distributions in the generator by $\pm 20\%$. The largest changes in the detection efficiencies, 1.6%, 0.5%, and 1.7% are taken as systematic uncertainties for $D^0 \to K^-\pi^+\eta'$, $D^0 \to K^0_S\pi^0\eta'$, and $D^+ \to K^0_S\pi^+\eta'$, respectively.

(ix) *MC statistics*: The uncertainties due to the limited MC statistics are 0.7%, 0.9%, and 0.7% for $D^0 \to K^-\pi^+\eta'$, $D^0 \to K^0_S\pi^0\eta'$, and $D^+ \to K^0_S\pi^+\eta'$, respectively.

(x) *Quoted branching fractions*: The uncertainties of the quoted branching fractions for $\eta' \to \pi^+\pi^-\eta$, $\eta \to \gamma\gamma$, $K^0_S \to \pi^+\pi^-$, and $\pi^0 \to \gamma\gamma$ are taken from the world average and are 1.6%, 0.5%, 0.07%, and 0.03% [1], respectively.

(xi) $D^0\bar{D}^0$ *mixing*: Because $D^0\bar{D}^0$ meson pair is coherently produced in $\psi(3770)$ decay, the effect of $D^0\bar{D}^0$ mixing on the branching fractions of neutral D meson decays is expected to be due to the next-to-leading-order of the $D^0\bar{D}^0$ mixing parameters x and y [17,18]. With $x = (0.32 \pm 0.14)\%$ and $y = (0.69^{+0.06}_{-0.07})\%$ from PDG [1], we conservatively assign 0.1% as the systematic uncertainty.

(xii) *DCS contribution*: Based on the world-averaged values of the branching fractions, the branching fraction ratios between the known DCS decays and the corresponding CF decays are in the range of (0.2–0.6)%. Therefore, we take the largest ratio 0.6% as a conservative estimation of the systematic uncertainty of the DCS effects.

The above relative systematic uncertainties are added in quadrature, and a total of 4.9%, 6.1%, 6.6%, 5.3%, and 6.0% for the measurements of $\mathcal{B}(D^0 \to K^-\pi^+\eta')$, $\mathcal{B}(D^0 \to K^0_S\pi^0\eta')$, $\mathcal{B}(D^+ \to K^0_S\pi^+\eta')$, $\mathcal{R}^0$, and $\mathcal{R}^+$, respectively, is obtained.

VII. SUMMARY AND DISCUSSION

Based on an analysis of an e^+e^- data sample with an integrated luminosity of 2.93 fb^{-1} collected at $\sqrt{s} =$ 3.773 GeV with the BESIII detector, we measure the branching fractions of hadronic D meson decays to

be: $\mathcal{B}(D^0 \to K^-\pi^+\eta') = (6.43 \pm 0.15_{\rm stat} \pm 0.31_{\rm syst}) \times 10^{-3}$, $\mathcal{B}(D^0 \to K^0_S\pi^0\eta') = (2.52 \pm 0.22_{\rm stat} \pm 0.15_{\rm syst}) \times 10^{-3}$, and $\mathcal{B}(D^+ \to K^0_S\pi^+\eta') = (1.90 \pm 0.17_{\rm stat} \pm 0.13_{\rm syst}) \times 10^{-3}$. The measured branching fraction of $D^0 \to K^-\pi^+\eta'$ is consistent with the previous result measured by CLEO [1,2], but improved with a factor of 4 in precision. The branching fractions of $D^0 \to K^0_S\pi^0\eta'$ and $D^+ \to K^0_S\pi^+\eta'$ are determined for the first time.

Using the measured branching fractions, we determine the ratios of branching fractions to be $\mathcal{R}^0 = 0.39 \pm 0.03_{\rm stat} \pm 0.02_{\rm syst}$. and $\mathcal{R}^+ = 0.30 \pm 0.03_{\rm stat} \pm 0.02_{\rm syst}$. $\mathcal{R}^0$ agrees well with the value 0.4 predicted by the SIM, but $\mathcal{R}^+$ significantly deviates from the expected value 0.9. This deviation may arise from a possible phase difference between two isospin states in the SIM [19]. In our analysis, we do not find an obvious K^* signal in the $K\pi$ invariant mass distributions, which is consistent with the predictions of small $D^0 \to \bar{K}^{*0}\eta'$ and $D^+ \to K^{*+}\eta'$ contributions [20–22].

Summing over the branching fractions of $D \to \bar{K}\pi\eta'$ decays and the other exclusive $D \to \eta' X$ decays in PDG [1], we obtain the sums of the branching fractions of all the exclusive $D^0 \to \eta' X$ and $D^+ \to \eta' X$ to be $(3.23 \pm 0.13)\%$ and $(1.06 \pm 0.07)\%$, respectively. They are consistent with the measured inclusive production $\mathcal{B}(D^0 \to \eta' X) = (2.48 \pm 0.27)\%$ and $\mathcal{B}(D^+ \to \eta' X) = (1.04 \pm 0.18)\%$ [23] within 2.5σ and 0.1σ, respectively. This excludes the possibility of additional exclusive $D \to \eta' X$ decay modes with large branching fractions.

ACKNOWLEDGMENTS

The BESIII collaboration thanks the staff of BEPCII and the IHEP computing center for their strong support. The authors are grateful to Fu-Sheng Yu, Jonathan L. Rosner, and Zhizhong Xing for helpful discussions. This work is supported in part by National Key Basic Research Program of China under Contract No. 2015CB856700; National Natural Science Foundation of China (NSFC) under Contracts Nos. 11335008, 11425524, 11475123, 11625523, 11635010, 11675200, 11735014, 11775230; the Chinese Academy of Sciences (CAS) Large-Scale Scientific Facility Program; the CAS Center for Excellence in Particle Physics (CCEPP); Joint Large-Scale Scientific Facility Funds of the NSFC and CAS under Contracts Nos. U1532257, U1532258, U1532101; CAS Key Research Program of Frontier Sciences under Contracts Nos. QYZDJ-SSW-SLH003, QYZDJ-SSW-SLH040; 100 Talents Program of CAS; INPAC and Shanghai Key Laboratory for Particle Physics and Cosmology; German Research Foundation DFG under Contracts Nos. Collaborative Research Center CRC 1044, FOR 2359; Istituto Nazionale di Fisica Nucleare, Italy; Koninklijke Nederlandse Akademie van Wetenschappen (KNAW) under Contract No. 530-4CDP03; Ministry of Development of Turkey under Contract No. DPT2006K-120470; National Science and Technology fund; The Swedish Research Council; U.S. Department of Energy under Contracts Nos. DE-FG02-05ER41374, DE-SC-0010118, DE-SC-0010504, DE-SC-0012069; University of Groningen (RuG) and the Helmholtzzentrum fuer Schwerionenforschung GmbH (GSI), Darmstadt.

[1] M. Tanabashi *et al.* (Particle Data Group), Phys. Rev. D **98**, 030001 (2018).
[2] M. Procario *et al.* (CLEO Collaboration), Phys. Rev. D **48**, 4007 (1993).
[3] M. Peshkin and J. L. Rosner, Nucl. Phys. **B122**, 144 (1977).
[4] M. Gronau and J. L. Rosner, Phys. Rev. D **79**, 074022 (2009).
[5] M. Ablikim *et al.* (BESIII Collaboration), Chin. Phys. C **37**, 123001 (2013); Phys. Lett. B **753**, 629 (2016).
[6] M. Ablikim *et al.* (BESIII Collaboration), Nucl. Instrum. Methods Phys. Res., Sect. A **614**, 345 (2010).
[7] S. Agostinelli *et al.* (GEANT4 Collaboration), Nucl. Instrum. Methods Phys. Res., Sect. A **506**, 250 (2003).
[8] S. Jadach, B. F. L. Ward, and Z. Was, Comput. Phys. Commun. **130**, 260 (2000); Phys. Rev. D **63**, 113009 (2001).
[9] E. A. Kureav and V. S. Fadin, Yad. Fiz. **41**, 733 (1985); [Sov. J. Nucl. Phys. **41**, 466 (1985)].
[10] E. Barberio and Z. Was, Comput. Phys. Commun. **79**, 291 (1994).
[11] D. J. Lange, Nucl. Instrum. Methods A **462**, 152 (2001); R. G. Ping, Chin. Phys. C **32**, 599 (2008).
[12] J. C. Chen, G. S. Huang, X. R. Qi, D. H. Zhang, and Y. S. Zhu, Phys. Rev. D **62**, 034003 (2000).
[13] H. Albrecht *et al.* (ARGUS Collaboration), Phys. Lett. B **241**, 278 (1990).
[14] M. Ablikim *et al.* (BESIII Collaboration), Chin. Phys. C **42**, 083001 (2018).
[15] M. Ablikim *et al.* (BESIII Collaboration), Phys. Rev. D **92**, 112008 (2015).
[16] M. Ablikim *et al.* (BESIII Collaboration), Eur. Phys. J. C **76**, 369 (2016); Chin. Phys. C **40**, 113001 (2016).
[17] Z. Z. Xing, Phys. Rev. D **55**, 196 (1997).
[18] D. M. Asner and W. M. Sun, Phys. Rev. D **73**, 034024 (2006); **77**, 019901(E) (2008).
[19] C. D. Lü, W. Wang, and F. S. Yu, Phys. Rev. D **93**, 056008 (2016).

[20] F. S. Yu, X. X. Wang, and C. D. Lü, Phys. Rev. D **84**, 074019 (2011).
[21] Q. Qin, H. N. Li, C. D. Lü, and F. S. Yu, Phys. Rev. D **89**, 054006 (2014).
[22] H. Y. Cheng, C. W. Chiang, and A. L. Kuo, Phys. Rev. D **93**, 114010 (2016).
[23] G. S. Huang *et al.* (CLEO Collaboration), Phys. Rev. D **74**, 112005 (2006).